論文 / 著書情報
Article / Book Information

Title	Experiment and modeling of translational dynamics of an oscillating bubble cluster in a stationary sound field
Author(s)	Naohiro Sugita, Keita Ando, Toshihiko Sugiura
Citation	Ultrasonics, Vol. 77, pp. 160-167
Pub. date	2017, 2
DOI	http://dx.doi.org/10.1016/j.ultras.2017.01.026
Creative Commons	See next page.
Note	This file is author (final) version.

License

Experiment and modeling of translational dynamics of an oscillating bubble cluster in a stationary sound field

Naohiro Sugita*, Keita Ando, Toshihiko Sugiura

Department of Mechnical Engineering, Keio University, Yokohama 2238522, Japan

Abstract

Translational motion of an oscillating bubble cluster under sound irradiation is studied experimentally and is modeled in the framework of the classical approach of Bjerknes. An experimental technique is proposed to observe bubble cluster formation and its translational dynamics interacting with wall boundaries due to the secondary Bjerknes force. The translational motion observed in the experiment is modeled by extending the classical theory of Bjerknes on single bubble; a bubble cluster is treated as a single bubble. The extended Bjerknes theory is shown to allow us to predict the overall trajectory of the cluster translating toward a wall of finite acoustic impedance by tuning acoustic energy loss at the wall. The drag force turns out to be unimportant for the translation of a millimeter-sized cluster that we observed.

Keywords: Bubble cluster dynamics, Sonication, Secondary Bjerknes force, High-speed imaging

1. Introduction

Growth of gas bubble nuclei under pressure fluctuations of the surrounding liquid and the subsequent oscillations are termed acoustic cavitation [1, 2, 3] and the subsequent dynamics of nucleated cavitation bubbles play an important role in many applications such as ultrasonic cleaning. This is due to the fact that

*Corresponding author
Email address: sugita@keio.jp (Naohiro Sugita)

inputted acoustic energy is effectively converted, through bubble oscillations in volume and translational instability of fissioned bubbles [4, 5], into mechanical energy within localized spots [6, 7]. Since oscillating and translating bubble clusters are accompanied frequently with violent collapses [8, 9], cavitation can give rise to undesired disruptive damage to surrounding solid materials (i.e., the so-called cavitation erosion).

Hydrodynamic interactive forces acting on oscillating bubbles were first studied by Bjerknes [10]. In the classical theory, two synchronously oscillating bubbles are subject to mutual attractive force, while two bubbles oscillating out-of-phase experience mutual repulsion. These kinds of mutual forces are known as secondary Bjerknes force and distinguished from the primary Bjerknes force that results from interaction with an external sound source. The magnitude of the secondary Bjerknes forces is proportional to the intensities of radial oscillation of each bubble and decays inversely with the square of the separation distance between the bubbles. It follows from the classical description that the secondary Bjerknes effect is mathematically equivalent to translational motion of one oscillating dipole subject to monopole radiation of the other.

More complicated behaviors of oscillating bubbles have been demonstrated theoretically by extending the classical theory of Bjerknes. One of earliest studies of Crum [11] assumed linear bubble oscillation and derived a simple expression of the secondary Bjerknes force after time-averaging over one oscillation period of the imposed sound frequency. Barbat et al. [12] modified Crum's formula by accounting for damped oscillation of spherical bubbles. The resulting phase shift between two resonant bubbles allowed a stable equilibrium point at which the sign of the secondary Bjerknes force changes. Oguz and Prosperetti [13] developed a set of ordinary differential equations for the coupled nonlinear dynamics between translational motion and bubble pulsation in an potential flow. Subsequently, Harkin et al. [14] classified patterns of translational motion of a couple of oscillating bubbles for the case of linear or weakly nonlinear forcing by means of the dynamical analysis of Oguz and Prosperetti [13], drawing a conclusion that the classical theory was valid only for a large separation distance

and weakly forced bubbles. Near-field interaction between bubbles is often results in nonspherical bubble deformation and there is thus a need to handle it using the boundary element method [15, 16]. Further extensions to the discussion on the secondary Bjerknes force between single bubbles have been proposed by several authors, which consider viscous liquid [17, 18], high-intensity sound pressure [19], multipole interaction or higher spherical harmonics [20], drag and history force on an oscillating bubble [21, 22, 23] and decoupling of the radial dynamics from the translational motion [24].

Validity of the time-averaged secondary Bjerknes force has been experimentally investigated for single bubbles in early works of Crum [11] and Barbat et al. [12], and more recently in the ultrasonic frequency range by Yoshida et al. [25] and Jiao et al. [26]. The coupled radial and translational model developed by Doinikov [19] was extended to microbubble-wall interaction by Xi et al. [27]. However, studies on the translational motion of an oscillating bubble "cluster" are rather limited, despite its practical importance. While the translational dynamics of cavitation clouds were recently investigated by Nowak and Mettin [28] and Johnston et al. [29], in an ultrasonic frequency range, the cluster dynamics could not be resolved in detail because of limitation in temporal and spatial resolution of the optical imaging. In this work, we aim to propose an experimental technique to resolve the dynamics of a translating bubble cluster under sonication and analyze the experimental observation with extended theory.

The goal of this study is to show the validity of the classical Bjerknes theory to a spherical cluster oscillation interacting with solid boundaries. In doing so, we develop a lower frequency vibration system [30, 31, 32] in order to resolve the entire picture of bubble cluster activities subject to a stationary sound field after the example of Nyborg and Rodgers [33] and Crum [11]. In what follows, we explain the experimental method and high-speed imaging of cluster events (bubble fission, clustering, cluster oscillation and translation, interaction with solid boundaries), present the temporal evolution of cluster size and translation, and finally analyze the translational dynamics with extended Bjerknes theory.

2. Experimental method

2.1. Experimental setup

The experimental setup is sketched in Fig. 1(a). A rectangular acrylic vessel (inside sizes: 50 mm × 50 mm × 100 mm, thickness: 5 mm) filled with tap water of 90 mm in height at the room temperature was fixed on a vibration generator (513-BS/Z08, EMIC Corp.). A vacuum pump (DAP-6D, ULVAC KIKO Inc.) was connected to the well-closed vessel through a valve in order to reduce the hydrostatic pressure in the vessel toward the vapor pressure. With the reduced ambient pressure, one can easily obtain cavitation even at low driving amplitude of the vibration generator [11]. Continuous sinusoidal excitation was input from a function generator (WF1973, NF Corp.) via a power amplifier (371-A, EMIC Corp.). The acceleration of the vessel in the vertical direction was measured by a accelerometer (710-D, EMIC Corp.) with a charge amplifier (6001-AHD/1NBD-1, EMIC Corp.), which was used to calculate the absolute liquid pressure. The gas pressure in the container was monitored by a pressure sensor (HAV-100KP-V, SENSEZ) attached on the top of the vessel. The absolute gas pressure remains approximately at 5.0 kPa under steady state operation of the vacuum pump. It turned out that the gas pressure is almost undisturbed, even with the presence of cavitation. It can therefore be assumed that the liquid pressure at the free surface is fixed at the gas pressure.

The recording system consists of a high-speed video camera (FASTCAM SA-5, Photron), a distortion-less macro lens (VS-LD50, VS Technology) combined with a 2.0× magnification converter lens (VS-2.0XV, VS Technology), and LED backlight (TS-LAX-RGB3, MeCan imaging). The spatial resolution of images was 41 μm per pixel. The recording frame rate of the high-speed camera was set at 10000 frame/s, which is sufficiently fast for image processing with the Fourier analysis. The exposure time of the camera was fixed to 0.1 ms.

2.2. Preparation of a bubble cluster

A millimeter-sized gas bubble as a cavitation nucleus was manually injected by a needle through a silicone plug of 4.5 mm in diameter, which was located

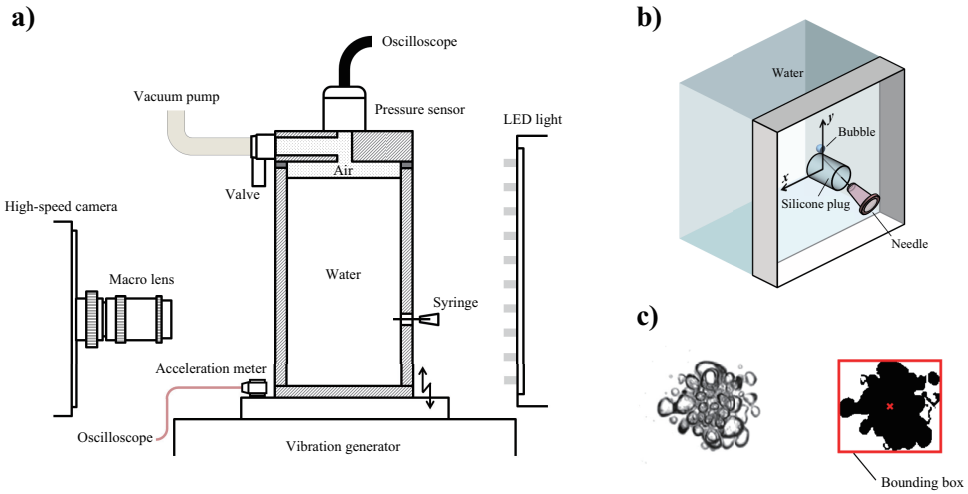

Figure 1: Schematic of (a) experimental setup, (b) an enlarged view of the silicone plug and needle and (c) comparison of a typical photographed image (left) and the image processing with a bounding box and its centroid (right).

at 30 mm above the vessel bottom and 25 mm away from the side walls. The bubble injection was sketched in Fig. 1(b). The diameter of the gas nucleus we obtained is approximately 1 mm. The side view of the bubble nucleus is shown in Fig. 2. The bubble remained attached to the wall surface unless the external driving force was imposed.

The periodic pressure field induced by the driving acceleration will follow a potential solution owing to the sufficiently long wave length and given in the form of [11, 33, 34]

$$p(h,t) = p_0 + \rho g h + \rho A \omega^2 h \sin \omega t \tag{1}$$

where h is the water depth measured from the free surface, p_0 is the static pressure at the free surface, ρ is the liquid density, g is the gravitational acceleration, A is the displacement amplitude of the vibration generator, and ω is the angular frequency of the vibration generator. Since p_0 reached 5.0 kPa after vacuuming, the hydrostatic pressure at the initial bubble position, at $h = 60$ mm ($\equiv h_0$), was reduced to 5.6 kPa. As a result of this pressure reduction, the injected bubble nucleus was subject to large amplitude oscillation and accompanying surface instability in the sub-kHz sound field even with a weak sound amplitude

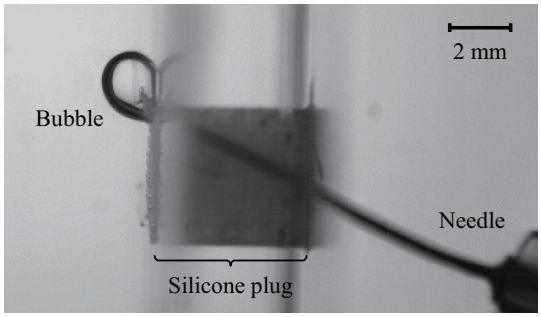

Figure 2: Sideview of an injected bubble nucleus corresponding to the schematic in Fig. 1(b).

$\rho A\omega^2 h$; this eventually leads to the formation of a collapsing bubble cluster. In fact, the displacement acceleration measured by the accelerometer was 29 m/s^2 for 625 Hz which yields sound amplitude of 1.9 kPa at $h = h_0$. However, further large driving amplitude gave rise to a large number of cavitation arising probably from pre-existing bubble nuclei at the container surface [35]. In order to observe only the motion of the injected bubble nucleus, the driving amplitude was set at sufficiently low levels to avoid such undesired cavitation events.

2.3. Image processing

The recorded images were analyzed using the image processing software (MATLAB, The Mathworks Inc.) function *graythresh* based on the binarization and thresholding technique of a recorded image sequence to 8-bit grayscale images. Figure 1(c) shows comparison between a captured image and a processed binary image with a bounding-box which encloses the contour of the cluster with the minimum area. The area of the bounding-box A_{box} and the coordinate of its centroid (X, Y) were computed for each recorded image. Here, we defined an area-equivalent mean radius R_{b} as

$$R_{\mathrm{b}} = \sqrt{\frac{\text{Area of the inscribed ellipse}}{\pi}} = \frac{\sqrt{A_{\mathrm{box}}}}{2}. \tag{2}$$

Temporal evolution of R_{b} was produced from the recorded image sequence, and Fourier spectrum of the time-radius curve was then calculated for the use of theoretical analysis. The transient velocity U in the x direction was calculated

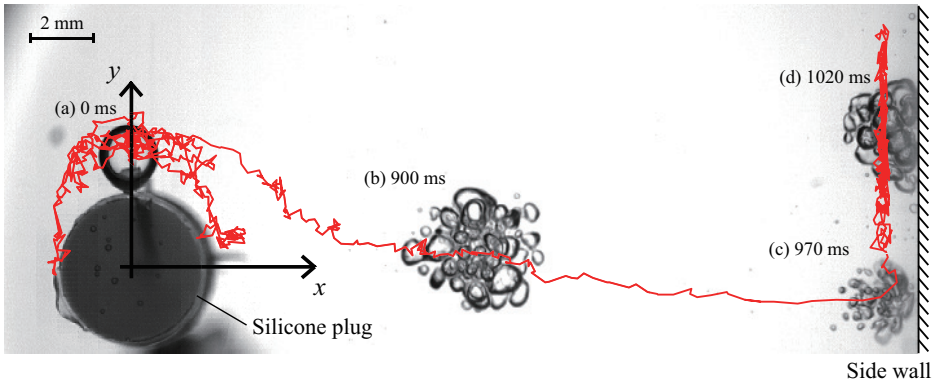

Figure 3: Trajectory of a cluster motion denoted by a red solid line. Representative pictures of the cluster are superimposed: (a) initial state, (b) collapse and fission, (c) jet formation and (d) oscillation in contact with the side wall. The injected bubble nucleus departs from the silicone plug and moves toward the right side wall.

by a simple central difference of the X–t curve where X stands for the geometric center of a bubble cluster. Before applying differentiation to compute the velocity, the X–t curve was smoothed using a moving average low-pass filtering based on the MATLAB function *filter*.

3. Experimental observation

3.1. Overview of bubble cluster dynamics

Figure 3 presents a representative example of cluster motion and its trajectory with the driving frequency 625 Hz. An initially injected bubble of R_b=1 mm departs from the silicone plug, oscillating in volume subject to the primary sound field. The bubble continuously collapses with the Rayleigh–Taylor-like surface instability and subsequent bubble fission [4], so that the bubble oscillates as a cluster of bubble fragments. It should be noted that the cluster motion occurs almost in the horizontal direction because the primary Bjerknes force counterbalances to the buoyant force in the vertical direction.

After some back-and-forth motion around the silicone plug, the bubble cluster goes straight to the right direction with increasing its translational velocity due to the secondary Bjerknes force that arises from the interaction with the side walls, as will be explained in Section 4. During the travel to the right

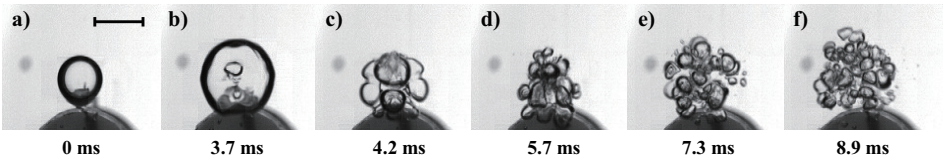

Figure 4: Snapshots of (a) the initial state, (b) maximum expansion, and (c-f) the consecutive collapse phases. The scale bar represents 2 mm.

side wall, the bubble cluster experienced kinds of phenomena shown in the following section, i.e., surface instability, bubble collapse and fission, coalescence, nonlinear oscillation, interaction with the wall boundaries.

3.2. Bubble collapse, fission and cluster oscillation

An image sequence of consecutive collapse phases is shown in Fig. 4. The dark circular structure seen beneath the bubble in the images is the upper part of the silicone plug. The initially spherical bubble reached a maximum radius $R_\mathrm{b} = 2.15$ mm, as seen in Fig. 4(b), after several driving periods. At the subsequent first collapse shown in Fig. 4(c), surface instability was developed, so that the bubble was split into fission fragments. The deformed bubble has lost the spherical symmetry, but the configuration of the fragments was almost exact line symmetry with respect to the vertical axis. This indicates that the primary

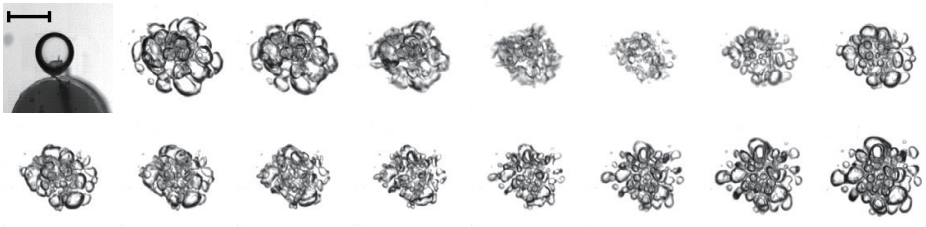

Figure 5: A typical image sequence of an oscillating bubble cluster driven at 625 Hz. The image sequence corresponds to one oscillation cycle of the imposed driving frequency. The scale bar represents 2 mm.

sound field does not have a significant pressure gradient in the x direction as described by Eq. (1). After the second collapse shown in Fig. 4(d), each tuft-like structure in Fig. 4(c) seems to be split again into a couple of daughter bubbles. Although the number of fission fragments was augmented and the size of bubble fragments was ununiformly distributed, the line symmetry was barely retained at this moment. During the third collapse, the fragmentation continued further as shown in Fig. 4(e), and much smaller bubbles were produced. As seen in Fig. 4(f), the bubble fragments tended to be single-sized after the forth collapse, and their oscillation phases were synchronized. At the subsequent collapses, the cluster looked very similar in a sense that the size and number of the bubble fragments remain at the same order, implying that fission and coalescence balance. The subsequent cluster oscillation for one driving period is shown in Fig. 5. The bubble cluster kept in contact with the back wall and slid across the contact surface with its shape remained nearly hemispherical.

Figure 6(a) shows the last 130 oscillation periods of the evolution of the cluster radius $R_{\rm b}$ before the bubble cluster crashed to the right side wall. The beginning of the external driving is set to $t = 0$. The volumetric response of the bubble cluster is found to be almost in a steady state during the observation. It should be noted that the interaction between the cluster and the right side wall comes into play just before the cluster reaches the wall; otherwise, the interaction does not play an important role in the volumetric oscillation. The bubble fragments remain gathered in a cluster. This is because attractive secondary Bjerknes forces, which acts on synchronously oscillating bubbles of the similar size, hold the bubble fragments closely together within the cluster. The evolution of the cluster radius in shorter time is shown in Fig. 6(b) and its Fourier spectrum (from 64 data points) is computed in Fig. 6(c). The fitting curve is reproduced using Eq. (5), to be presented in the following section, where nonlinear components up to the third harmonic δ_3 are considered. It is clearly seen that there arises nonlinear resonance in the oscillation; the second superharmonic at 1250 Hz (i.e., twice the driving frequency) is notably evident. It follows that the resonant frequency of the cluster oscillation would lie around

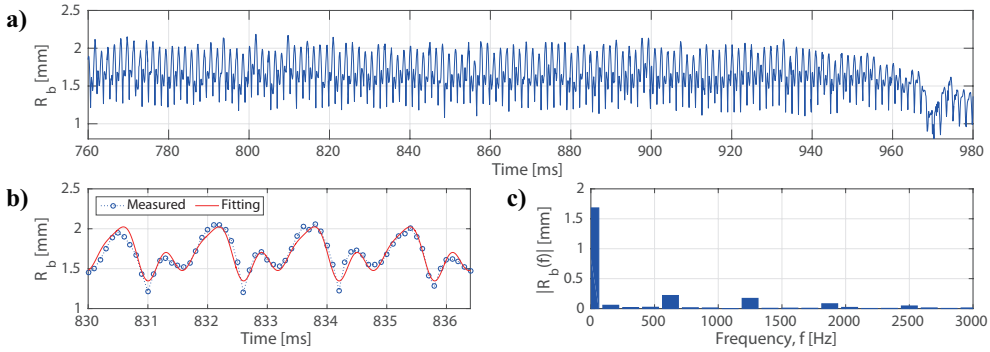

Figure 6: The results of image processing. (a) R_{b}–t curve, (b) R_{b}–t curve (enlarged) and (c) its Fourier spectrum. The fitting curve in (b) was reproduced using the frequency component up to the third harmonics of (c).

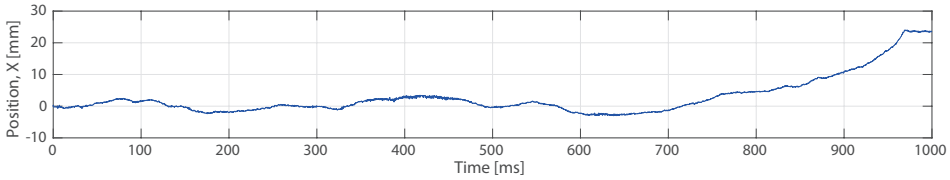

Figure 7: The temporal evolution of the cluster position.

1250 Hz. If the damping effect is small, resonant frequency of a spherical gas bubble is given by the Minnaert frequency, ω_M [36]. The formula of the natural frequency can be extended to the case of a spherical bubble cluster that consists of single-sized bubbles [37, 38] and is given by

$$\omega_c = \frac{1}{a_0}\sqrt{\frac{3\gamma p_0 + \frac{2S}{a_0}(3\gamma - 1)}{\rho\left(1 + \frac{N^{1/3}a_0}{R_0}\left(N^{2/3} - 1\right)\right)}} < \omega_M. \tag{3}$$

where R_0 is the equilibrium cluster radius, a_0 is the equilibrium radius of bubbles in the cluster, γ is the ratio of the specific heats of the bubble contents and S is the surface tension. Equation (3) is reduced to the Minnaert frequency when $N = 1$ and the surface tension is neglected. Calculating with $\gamma = 1.4$ (for air), $S = 0.073$ N/m, $R_0 = 1.6$ mm and $p_0 - p_v \sim 3$ kPa offers a reasonable estimation of a_0, given the cluster's resonance frequency $\omega_c = 2\pi \times 1250$ rad/s; $a_0 = 0.58$ mm, 0.35 mm, 0.17 mm and 0.081 mm, re-

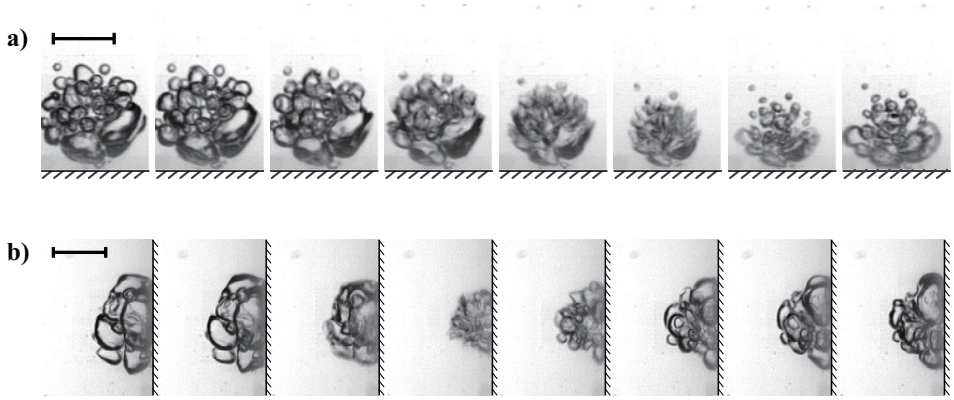

Figure 8: An image sequence of (a) the jet-like motion and (b) spherical oscillation in contact with the right side wall driven at 625 Hz. The scale bar represents 2 mm.

spectively, for $N = 1,\ 10,\ 100$ and 1000. In the particular example of our experiment in Fig. 3, the cluster dynamics are tuned to be under resonance at twice the driving frequency. Indeed, we also observed cluster oscillation under primary resonance (i.e., resonance at an imposed frequency) by lowering the driving sound frequency, which consists of a small number of N but arising from similar R_0, leading to larger bubble fragments than that of Fig. 4. The result is consistent with the above discussion in that one obtains a smaller resonant frequency from Eq. (3) for the case of larger a_0.

3.3. Interaction with wall boundaries

The trajectory of the cluster center is shown in Fig. 7. The cluster stayed around the plug until $t = 760$ ms. After that, the cluster began traveling toward the right side wall subjected to the secondary Bjerknes force exerted from the wall. The direction of movement depends not only on the initial position, but also the detuning of the vibrating system and randomness of the fission process. The impact on the right wall (located at $x = 25$ mm) occurred approximately at $t = 970$ ms.

The oscillating bubble cluster radiates secondary pressure field, p_{rad}, which

reflects on the side walls and forms a pressure gradient at the cluster normal to the wall, $\partial p_{\mathrm{rad}}/\partial x$. The cluster with volume $V(t)$ in the pressure gradient experienced an instantaneous force, $-V(t)\partial p_{\mathrm{rad}}/\partial x$. Since this force is composed of a product of oscillating components, time-averaging of this force leads to mean motion of the cluster. The direction of the force is determined by phase angle between the cluster oscillation and the reflected wave. It is instructive to note that in the y direction, buoyant force counterbalanced to the Bjerknes force due to the primary sound field induced by the driving acceleration (strictly, interaction with the bottom wall and top surface contribute to the force balance). This allowed the cluster to move almost in the horizontal direction. The translational dynamics in the x direction will be modeled and examined in Section 4.

At the final stage of the wall impact, we observed a jet-like motion of the bubble cluster shown in Fig. 8(a), which is similar to the phenomenon of a single bubble near a wall boundary; asymmetric bubble collapse leads to formation of a liquid jet directed toward the wall [8, 7]. The interaction between larger bubbles in the cluster and the wall boundary became much stronger than that of bubble-bubble interaction; smaller bubbles were no longer able to follow up the fast motion and left behind the cluster. After the impact on the wall, side view of cluster oscillation were captured at the corner of the container shown in Fig. 8(b). Once the cluster was attached to wall surface, the shape of the cluster remained almost hemispherical during oscillation, meaning that the boundary layer at the side wall does not have an impact on the cluster dynamics.

4. Modeling of the translational motion

4.1. Secondary Bjerknes force

Figure 9 illustrates the top view of the vibrating water vessel. The separation between the left and right side walls is $2L$, and the center of a (hemispherical) bubble cluster in the x direction is denoted by X and is initially set at the middle of the side walls (i.e., $-L < X < L$). Here, we consider fictitious bubble clusters that are mirrored with respect to the left and right side walls;

the mirrored clusters are set at $2\,(L+X)$ and $2\,(L-X)$ away from the original cluster. With these mirrored clusters, we aim to model the interaction of the oscillating bubble cluster of our target with the side walls.

We treat the acrylic side wall as an elastic boundary and assume that the secondary sound field induced by oscillation of a bubble cluster is spherically symmetric. Since the interaction between the bubble cluster and the plane boundaries is equivalent to monopole interaction with its images, the gradient of the radiation pressure at distance l away from the center of an oscillating cluster is described by [3]

$$\left.\frac{\partial p_a}{\partial r}\right|_{r=l} = -\frac{\rho\left(R^2\ddot{R}+2R\dot{R}^2\right)}{l^2} \tag{4}$$

where dots denote time derivative, r is the coordinate in the spherical coordinate, ρ is the (constant) density of the liquid, R is the time-varying cluster radius, and l is the distance to measurement point from the cluster center. For clarity, we account only for the adjacent two images in the x direction while neglecting any higher-order corrections. Since we will below introduce simplifications in fluid dynamics modeling of cluster translation, higher-order corrections are expected to be minor.

The radial oscillation of a spherical cluster is now expanded as Fourier series:

$$R(t) = R_0\left[1+\delta_0+\sum_{k=1}^{n}\delta_k\sin(k\omega t+\phi_k)\right] \tag{5}$$

where R_0 is the radius of the (initially injected) bubble nucleus, ω is the angular frequency of the primary sound field induced by the external driving, and δ_k and ϕ_k $(k=0,1,\ldots,n)$ are, respectively, the small amplitude and the phase angle of frequency component k. Here, the mean radius of the cluster, R_c, is defined as a time average of $R(t)$ by

$$R_c = R_0\,(1+\delta_0)\,. \tag{6}$$

Since the primary sound field governed by Eq. (1) is a function of $y\,(=h_0-h)$ and has no significant pressure gradient in the x direction, the force acting on

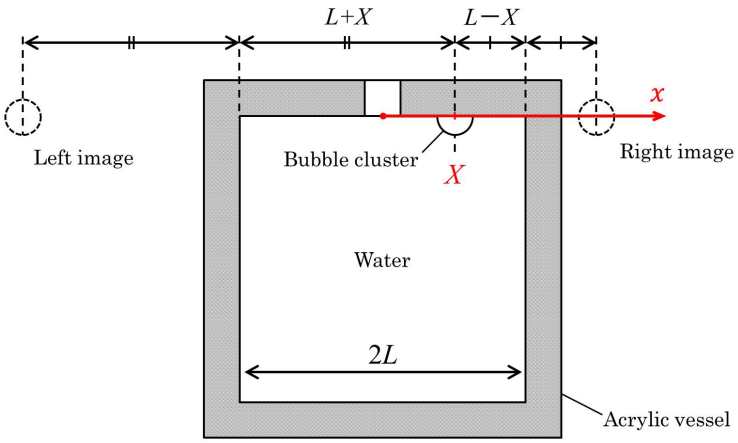

Figure 9: Schematic of the water vessel (top view). X and $2L$ denote the center of a hemispherical bubble cluster and the separation distance between the left and right side walls, respectively. The bubble cluster is mirrored with respect to the left and right side walls; the mirrored clusters are set at $2\,(L+X)$ and $2\,(L-X)$ away from the original cluster.

the cluster is only due to the reflected pressure wave from the side walls [11]. Therefore, the pressure gradient of the reflected wave at the center of the bubble cluster is approximated by

$$\left.\frac{\partial p_a}{\partial x}\right|_{x=X} = -\left[\frac{\rho R_c^2 \ddot{R}}{4(L-X)^2} - \frac{\rho R_c^2 \ddot{R}}{4(L+X)^2}\right] Q \tag{7}$$

where the complex quantity Q represents acoustic energy loss through transmission to the side walls of finite acoustic impedance. To be simple, the loss Q is assumed to be constant regardless of the frequency. The time-averaged Bjerknes force (of the second kind) in the x direction is obtained as a function of position X,

$$F_B(X) = -\left\langle V(t)\frac{\partial p_a(X,t)}{\partial x}\right\rangle \tag{8}$$

where $\langle\cdot\rangle$ denotes a time averag over the driving period $2\pi\omega^{-1}$ and $V(t) = (4\pi/3)R^3(t)$ is the volume of the spherical bubble cluster. Substituting Eq. (7) into Eq. (8) leads to

$$F_B(X) = 2\pi\rho\omega^2 R_c^6 \Delta^2 \left[\frac{1}{4(L-X)^2} - \frac{1}{4(L+X)^2}\right] \Re[Q] \tag{9}$$

where $\Re$ denotes the real part and

$$\Delta = \frac{1}{1+\delta_0}\left[\sum_{k=1}^{3} k^2 \delta_k^2\right]^{\frac{1}{2}}. \tag{10}$$

Here, higher nonlinear corrections of the order $O(\delta_1^i \delta_2^j \delta_3^k)$ $(i+j+k \geq 3;\ i,\ j$ and k are integers$)$ are neglected in Eq. (9). We note that a long-term behavior of the translation of an oscillating bubble cluster arises from quadratic nonlinear terms $O(k^2)$ in the expression of the Bjerknes force F_B.

4.2. Translational motion of the bubble cluster

The translation of the bubble cluster may be described by

$$m\frac{dU}{dt} = F_B + F_D + F_A \tag{11}$$

where U is the translational velocity and m is the mass within the cluster. Since the gas phase is essentially massless, the cluster mass is approximated by

$$m = \frac{4}{3}\pi\rho R_c^3 (1-\alpha), \tag{12}$$

where α is the so-called void fraction (i.e., the volume fraction of the gas phase). The case of no bubbles is represented by $\alpha = 0$. The added force, F_A, arising from unsteadiness is calculated by [12]

$$F_A = \frac{2}{3}\pi\rho R_c^3 \frac{dU}{dt}, \tag{13}$$

where $(2/3)\pi\rho R_c^3$ means the added mass. The drag force acting on the bubble cluster is given by the Levich's formula [19],

$$F_D(U) = -12\pi\mu R_c U \tag{14}$$

where μ is the liquid viscosity. We will show that the contribution of the drag force have negligible impact on the translation. Because of the assumption of small-amplitude oscillations, the cluster radius is evaluated as the undisturbed constant R_c in Eqs. (12) to (14) [24].

Table 1: The cluster radius R_c and oscillation amplitudes δ_k determined by the experimentally obtained Fourier spectrum. The radius of the (initially injected) bubble nucleus is $R_0 = 1.01$ mm. The imposed sound frequency is 625 Hz.

R_c[mm]	δ_0	δ_1	δ_2	δ_3
1.68	0.665	0.216	0.169	0.0802

The dimensionless variables (superscripted by asterisks) are defined as

$$U^* = \frac{U}{\omega L}, \quad X^* = \frac{X}{L}, \quad t^* = \omega t. \tag{15}$$

Substituting Eqs. (15) into Eq. (11) leads to the dimensionless form

$$\frac{dU^*}{dt^*} = B\left[\frac{1}{(1-X^*)^2} - \frac{1}{(1+X^*)^2}\right] - CU^*. \tag{16}$$

There arise the two dimensionless parameters

$$B = \frac{3}{4m^*}\left(\frac{R_c}{L}\right)^3 \Delta^2 \Re[Q], \quad C = \frac{3}{4m^*}\frac{R_c}{L}\frac{48}{\mathrm{Re}}. \tag{17}$$

where m^* is the dimensionless mass that consists of the cluster mass and the added mass is given by

$$m^* = 3 - 2\alpha. \tag{18}$$

For the case of a single bubble (not a cluster) with $\alpha = 1$, this reduces to $m^* = 1$. Note that B presents intensity of the acoustic radiation from the bubble cluster including the acoustic energy loss, and C is the drag force where $\mathrm{Re} = (2R_c)^2 \omega \nu^{-1}$ is Reynolds number from the cluster translation. For the inviscid case ($C = 0$), one can explicitly derive the exact solution of Eq. (16). Multiplying the both side of Eq. (16) by U^* and integrating with initial conditions (X_0, U_0) yield

$$U^{*2} = \left(U_0^{*2} - \frac{4B}{1-X_0^{*2}}\right) + \frac{4B}{1-X^{*2}}. \tag{19}$$

For reference, the eigenvalue analysis of the dynamical system described by Eq. (16) is presented in Appendix A.

5. Comparison to the experimental result

With the model we proposed in the previous section, we now try to replicate the cluster translation observed in Fig. 3. The mean radius R_c and oscillation amplitudes δ_k are determined from the Fourier spectrum in Fig. 6(c):

$$R_c = |R_{\rm b}(f)|_{f=0} \tag{20}$$

$$\delta_k = |R_{\rm b}(f)|_{f=\frac{\omega}{2\pi}\times k} \tag{21}$$

where k takes 1, 2, or 3. The computed values of Eqs. (20) and (21) are summarized in Table 1. For water, we have $\rho = 1000$ kg/m^3 and $\mu = 0.001$ Pa·s. The initial position and velocity of the bubble cluster are set, respectively, at $X_0 = 4$ mm and $U_0 = 0.01$ m/s; the simulation result is not altered significantly by slight changes in the values of X_0 and U_0. The void fraction is approximated by

$$\alpha \approx \left(\frac{R_0}{R_c}\right)^3 = 0.27 \tag{22}$$

Comparison of the temporal evolution of X between the experiment and the model is made in Fig. 10 where the parameter for the acoustic energy loss is set at $\Re[Q] = 0.22$. The maximum particle Reynolds number defined as $\mathrm{Re}_U = 2R_cU\nu^{-1}$ is approximately 1900 for $U_{\max} = 0.576$ m/s at $X = 23$ mm. The computed curve fits well to the experiment except near the cluster-wall collision. It should be noted, however, that higher-order nonlinear corrections neglected in the present model may be needed for the short-distance interaction; the model overestimates the translational velocity as the separation distance decreases. We also note that the evaluation of the drag force acting on the cluster is unimportant, for a change in the computation is insignificant between the viscous and inviscid cases; the translational motion is determined mainly by the secondary Bjerknes force and the inertia of the oscillating bubble cluster in this particular example.

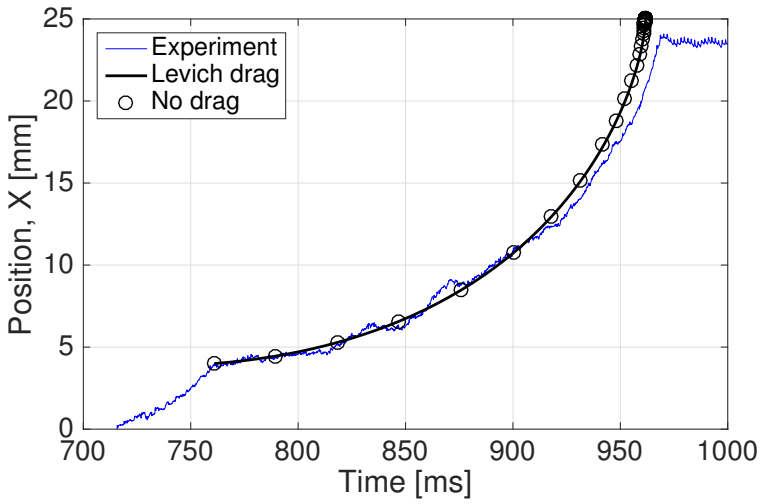

Figure 10: Comparison between the experiment and simulations: the results of the temporal evolution of the cluster position. The parameter for the acoustic energy loss is set at $\Re[Q] = 0.22$.

6. Conclusion

An experimental technique was developed to observe translation of a bubble cluster oscillating under a stationary sound field and the translational dynamics were modeled by simply extending the theory of Bjerknes. A gas bubble nucleus showed nonlinear oscillation in a low-frequency vibrating vessel and eventually leads to fission into bubble fragments. The bubble cluster showed translation toward the side wall. We explained the cluster translation as a result of the interaction with imaginary bubbles located at the opposite side of the side walls. The interaction was modeled by applying the Bjerknes theory of the second kind where the cluster is treated as a single bubble, while acoustic energy loss at the elastic wall was treated as a tuning parameter. We showed that the cluster translation observed in the experiment can be predicted properly by solving the equation of the cluster motion coupled with extended Bjerknes theory. It is concluded that the cluster translation in the present experiment is determined mainly by the secondary Bjerknes force and the cluster inertia.

Acknowledgment

We acknowledge Tatsuya Yamashita and Takehiro Nakajima for their help in data processing and thank Takeshi Nagasawa for his support on experiment. This work was supported by Keio University Doctorate Student Grant-in-Aid Program 2015.

Appendix A. Eigenvalue analysis

The translational dynamics described by Eq. (16) has only one equilibrium point $(X^*_{\rm st}, U^*_{\rm st}) = (0, 0)$, which is a stationary solution of the system. Perturbation of (X^*, U^*) from the fixed point is denoted by $(\delta x, \delta u)$, and the linear truncation of Eq. (16) is obtained in the form of

$$\frac{d}{dt^*}\begin{pmatrix} \delta x \\ \delta u \end{pmatrix} = \begin{bmatrix} 0 & 1 \\ -4B & -C \end{bmatrix}\begin{pmatrix} \delta x \\ \delta u \end{pmatrix} \tag{.1}$$

after the transformation with $X^* = X^*_{\rm st} + \delta x$ and $U^* = U^*_{\rm st} + \delta u$. The eigenvalues of the system are

$$\lambda = \frac{-C \pm \sqrt{C^2 + 16B}}{2}. \tag{.2}$$

The bifurcation structure can be understood in B–C plain and is divided into three regions. The stability of $(X^*_{\rm st}, U^*_{\rm st})$ is determined only by the sign of B as explained below. When $B > 0$, the equilibrium point is unstable (saddle point) because of a positive real eigenvalue. This indicates that the oscillating bubble can not stay away from the both side walls, leading to the attractive motion toward the walls. When B is negative, the equilibrium point is stable node or spiral depending on the magnitude of C, which is assumed positive real in this study. If $B < 0$ and C is small enough to satisfy $C^2 + 16B < 0$, the system presents damped oscillatory motion around the stable equilibrium point due to the complex eigenvalues. Increasing C causes qualitative change of the bubble behavior from damped oscillation to asymptotic motion to the equilibrium point. The sign of B depends on the acoustic impedance of the wall boundary, the separation distance and the imposed sound frequency [39].

References

[1] R. Apfel, Acoustic cavitation inception, Ultrasonics 22 (4) (1984) 167–173.

[2] E. Neppiras, Acoustic cavitation series: part one: Acoustic cavitation: an introduction, Ultrasonics 22 (1) (1984) 25–28.

[3] C. E. Brennen, Cavitation and bubble dynamics, Cambridge University Press, 2013.

[4] C. E. Brennen, Fission of collapsing cavitation bubbles, Journal of Fluid Mechanics 472 (2002) 153–166.

[5] C. F. Delale, M. Tunç, A bubble fission model for collapsing cavitation bubbles, Physics of Fluids (1994-present) 16 (11) (2004) 4200–4203.

[6] D. Krefting, R. Mettin, W. Lauterborn, High-speed observation of acoustic cavitation erosion in multibubble systems, Ultrasonics Sonochemistry 11 (3) (2004) 119–123.

[7] T.-H. Kim, H.-Y. Kim, Disruptive bubble behaviour leading to microstructure damage in an ultrasonic field, Journal of Fluid Mechanics 750 (2014) 355–371.

[8] W. Lauterborn, H. Bolle, Experimental investigations of cavitation-bubble collapse in the neighbourhood of a solid boundary, Journal of Fluid Mechanics 72 (02) (1975) 391–399.

[9] W. Kreider, L. A. Crum, M. R. Bailey, O. A. Sapozhnikov, Observations of the collapses and rebounds of millimeter-sized lithotripsy bubbles, The Journal of the Acoustical Society of America 130 (5) (2011) 3531–3540.

[10] V. F. K. Bjerknes, Fields of force, Columbia University Press, 1906.

[11] L. A. Crum, Bjerknes forces on bubbles in a stationary sound field, The Journal of the Acoustical Society of America 57 (6) (1975) 1363–1370.

[12] T. Barbat, N. Ashgriz, C.-S. Liu, Dynamics of two interacting bubbles in an acoustic field, Journal of Fluid Mechanics 389 (1999) 137–168.

[13] H. N. Oguz, A. Prosperetti, A generalization of the impulse and virial theorems with an application to bubble oscillations, Journal of Fluid Mechanics 218 (1990) 143–162.

[14] A. Harkin, T. J. Kaper, A. Nadim, Coupled pulsation and translation of two gas bubbles in a liquid, Journal of Fluid Mechanics 445 (2001) 377–411.

[15] N. A. Pelekasis, J. A. Tsamopoulos, Bjerknes forces between two bubbles. part 1. response to a step change in pressure, Journal of Fluid Mechanics 254 (1993) 467–499.

[16] N. A. Pelekasis, J. A. Tsamopoulos, Bjerknes forces between two bubbles. part 2. response to an oscillatory pressure field, Journal of Fluid Mechanics 254 (1993) 501–527.

[17] A. A. Doinikov, Viscous effects on the interaction force between two small gas bubbles in a weak acoustic field, The Journal of the Acoustical Society of America 111 (4) (2002) 1602–1609.

[18] N. A. Pelekasis, A. Gaki, A. Doinikov, J. A. Tsamopoulos, Secondary bjerknes forces between two bubbles and the phenomenon of acoustic streamers, Journal of Fluid Mechanics 500 (2004) 313–347.

[19] A. A. Doinikov, Translational motion of a spherical bubble in an acoustic standing wave of high intensity, Physics of Fluids 14 (4) (2002) 1420–1425.

[20] A. Doinikov, S. Zavtrak, On the mutual interaction of two gas bubbles in a sound field, Physics of Fluids (1994-present) 7 (8) (1995) 1923–1930.

[21] I. Kang, L. Leal, The drag coefficient for a spherical bubble in a uniform streaming flow, Physics of Fluids (1958-1988) 31 (2) (1988) 233–237.

[22] J. Magnaudet, D. Legendre, The viscous drag force on a spherical bubble with a time-dependent radius, Physics of Fluids (1994-present) 10 (3) (1998) 550–554.

[23] A. J. Reddy, A. J. Szeri, Coupled dynamics of translation and collapse of acoustically driven microbubbles, The Journal of the Acoustical Society of America 112 (4) (2002) 1346–1352.

[24] D. Krefting, J. O. Toilliez, A. J. Szeri, R. Mettin, W. Lauterborn, Translation of bubbles subject to weak acoustic forcing and error in decoupling from volume oscillations, The Journal of the Acoustical Society of America 120 (2) (2006) 670–675.

[25] K. Yoshida, T. Fujikawa, Y. Watanabe, Experimental investigation on reversal of secondary bjerknes force between two bubbles in ultrasonic standing wave, The Journal of the Acoustical Society of America 130 (1) (2011) 135–144.

[26] J. Jiao, Y. He, S. E. Kentish, M. Ashokkumar, R. Manasseh, J. Lee, Experimental and theoretical analysis of secondary bjerknes forces between two bubbles in a standing wave, Ultrasonics 58 (2015) 35–42.

[27] X. Xi, F. Cegla, R. Mettin, F. Holsteyns, A. Lippert, Collective bubble dynamics near a surface in a weak acoustic standing wave field, The Journal of the Acoustical Society of America 132 (1) (2012) 37–47.

[28] T. Nowak, R. Mettin, Unsteady translation and repetitive jetting of acoustic cavitation bubbles, Physical Review E 90 (3) (2014) 033016.

[29] K. Johnston, P. Prentice, B. Gerold, Cavitation cloud translation in focused ultrasound, in: Ultrasonics Symposium (IUS), 2014 IEEE International, IEEE, 2014, pp. 61–64.

[30] G. Jameson, J. Davidson, The motion of a bubble in a vertically oscillating liquid: theory for an inviscid liquid, and experimental results, Chemical Engineering Science 21 (1) (1966) 29–34.

[31] M. Baird, Behavior of gas bubbles in a vertically vibrating liquid column, The Canadian Journal of Chemical Engineering 46 (6) (1968) 482–482.

[32] S. Sudo, H. Hashimoto, Unsteady pressure response of a liqud in a cylindrical container subject to vertical vibration, JSME international journal. Ser. 2, Fluids engineering, heat transfer, power, combustion, thermophysical properties 31 (2) (1988) 227–233.

[33] W. Nyborg, A. Rodgers, The motion of liquid inside a closed vibrating vessel, Biotechnology and Bioengineering 9 (2) (1967) 235–256.

[34] V. Sorokin, I. Blekhman, V. Vasilkov, Motion of a gas bubble in fluid under vibration, Nonlinear Dynamics 67 (1) (2012) 147–158.

[35] A. A. Atchley, A. Prosperetti, The crevice model of bubble nucleation, The Journal of the Acoustical Society of America 86 (3) (1989) 1065–1084.

[36] T. Leighton, The acoustic bubble, Academic press, 2012.

[37] R. Nigmatulin, I. S. Akhatov, N. Vakhitova, E. S. Nasibullayeva, Dynamics of bubble clusters, in: NONLINEAR ACOUSTICS AT THE TURN OF THE MILLENNIUM: ISNA 15, 15th International Symposium, Vol. 524, AIP Publishing, 2000, pp. 455–458.

[38] E. S. Nasibullaeva, I. Akhatov, Bubble cluster dynamics in an acoustic field, The Journal of the Acoustical Society of America 133 (6) (2013) 3727–3738.

[39] U. Ingard, On the reflection of a spherical sound wave from an infinite plane, The Journal of the Acoustical Society of America 23 (3) (1951) 329–335.